Large Eddy Simulation of the Ocean Mixed Layer: The Effects of Wave Breaking and Langmuir Circulation

YIGN NOH AND HONG SIK MIN

Department of Atmospheric Sciences, Yonsei University, Seoul, Korea

SIEGFRIED RAASCH

Institute of Meteorology and Climatology, University of Hannover, Hanover, Germany

(Manuscript received 17 February 2003, in final form 9 September 2003)

ABSTRACT

Large eddy simulation (LES) of the ocean mixed layer was performed in which both wave breaking and Langmuir circulation are realized. Wave breaking was represented by random forcing consistent with the observed near-surface turbulence, and Langmuir circulation was realized by the Craig–Leibovich vortex force. High-resolution simulations were carried out using parallel computing with or without each contribution, wave breaking and Langmuir circulation, with an aim to clarify their respective roles in the ocean mixed layer. The effects of wave breaking were found to be mainly limited to the near-surface zone of the upper few meters. Langmuir circulations below it are not significantly modified, although they become somewhat weakened and less coherent. Under the influence of wave breaking, however, the turbulence production in the upper-ocean mixed layer becomes dominated by the turbulent kinetic energy flux, contrary to the case of the atmospheric boundary layer where it is dominated by shear production. The comparison of the results from the LES and the ocean mixed layer model also reveals the significances of wave breaking and Langmuir circulation in the vertical mixing process of the ocean mixed layer.

1. Introduction

The most significant characteristic of the ocean mixed layer in contrast to the atmospheric boundary layer is the presence of wave breaking and Langmuir circulation at the free surface. Breaking of surface waves generates large amounts of small-scale turbulence near the sea surface, and the interaction between the wind-driven surface shear and the Stokes drift of surface waves generates Langmuir circulations that are large circulation cells aligned in the wind direction (see, e.g., Leibovich 1983; Melville 1996).

Recent measurements revealed that wave breaking causes the dissipation rate of turbulence ε near the sea surface to be ~two orders larger than expected from the classical logarithmic boundary layer near the rigid surface, such as in the atmospheric boundary layer (Gargett 1989; Agrawal et al. 1992; Anis and Moum 1995; Drennan et al. 1996; Melville 1996). Wave breaking also causes the roughness length scale at the sea surface to be in the range of 0.1–8 m, which is much larger than that of the atmospheric boundary layer (Agrawal et al. 1992; Craig and Banner 1994; Drennan et al. 1996; Gemmrich and Farmer 1999).

Based on observation data, Craig and Banner (1994) suggested that in the near-surface layer influenced by wave breaking the turbulence production is dominated by the turbulent kinetic energy (TKE) flux rather than the mean shear. It was also supported by the analysis of the TKE budget from an ocean mixed layer model including the effects of wave breaking (Noh 1996). Hence, in the upper part of the ocean mixed layer a balance between TKE flux and dissipation is reached, and it leads to a relation for the variation of ε with depth z as $\varepsilon \sim z^{-n}$ with $n \sim 2$–4, in contrast to the wall boundary layer scaling such as $\varepsilon \sim z^{-1}$ (Agrawal et al. 1992; Craig and Banner 1994; Anis and Moum 1995; Drennan et al. 1996; Terray et al. 1996). The scaling of the wall boundary layer may be recovered below these depths.

There have been many reported observations of Langmuir circulation since Langmuir (1938) (Weller and Price 1988; Smith 1992; Plueddemann et al. 1996). Langmuir circulations are typically generated when the wind speed is larger than 3 m s^{-1}, and the downward vertical velocity below the convergence region increases with the wind speed, sometimes exceeding 0.2 m s^{-1} (Leibovich 1983; Weller and Price 1988; Plueddemann

Corresponding author address: Yign Noh, Department of Atmospheric Sciences, Yonsei University, 134 Shinchon-dong, Seodaemun-gu, Seoul 120-749, Korea.
E-mail: noh@atmos.yonsei.ac.kr

et al. 1996). Surface convergence lines extend up to 2 km in length, and the spacing between cells ranges from two to hundreds of meters. Sonar observation of bubble clouds produced by breaking wind waves manifested the streaks with a variety of scales, merging at characteristic Y junctions to form large circulation cells (Zedel and Farmer 1991; Thorpe 1992). The streaks are usually aligned downwind and propagate to the right of the main wind direction, implying the Coriolis effect. Weller and Price (1988) also observed that Langmuir circulation is able to destroy the near-surface stratification formed under diurnal heating, and its magnitude becomes much weaker in the lower half of the ocean mixed layer.

The prevailing theory of Langmuir circulation is that of Craik and Leibovich (1976), which describes the formation of Langmuir circulation in terms of an instability brought on by the interaction of the Stokes drift with the wind-driven surface shear current. The instability is initiated by an additional ''vortex force'' term in the momentum equation as $\mathbf{u}_s \times \boldsymbol{\omega}$, where $\mathbf{u}_s$ is Stokes drift velocity and $\boldsymbol{\omega}$ is vorticity.

Assuming a constant frictional velocity u_*, for surface waves with a characteristic wavenumber k and the Stokes drift velocity at the surface U_s, the occurrence of Langmuir circulations in a laminar flow with constant viscosity ν is determined by the Langmuir number La (Leibovich 1977) defined by

$$\mathrm{La} = \left(\frac{\nu k}{u_*}\right)^{3/2}\left(\frac{u_*}{U_s}\right)^{1/2}, \tag{1}$$

which represents a balance between the rate of diffusion of streamwise vorticity and the rate of production of streamwise vorticity by vortex stretching accomplished by the Stokes force.

In contrast, McWilliams et al. (1997) suggested a turbulent Langmuir number La_t as the relevant parameter in the turbulent ocean mixed layer as

$$\mathrm{La}_t = (u_*/U_s)^{1/2}. \tag{2}$$

Considering the strong turbulence near the surface generated by wave breaking and the large-scale eddies associated with Langmuir circulations, it is natural to suspect that both wave breaking and Langmuir circulation may play important roles in the vertical mixing process in the ocean mixed layer. Nonetheless, their effects have not been taken into consideration in most ocean mixed layer models developed earlier (e.g., Kraus and Turner 1967; Mellor and Durbin 1975; Niiler and Kraus 1977; Price et al. 1986; Gaspar 1988; Large et al. 1994).

Recently, efforts have been made to incorporate these effects into the ocean mixed layer models; for example, Noh and Kim (1999), D'Alessio et al. (1998), and Burchard (2001) for the effects of wave breaking and Li and Garrett (1997), D'Alessio et al. (1998), and McWilliams and Sullivan (2000) for the effects of Langmuir circulation. In particular, Noh (1996) showed that the inclusion of turbulence generated by wave breaking is indispensable for the formation of a diurnal or seasonal thermocline under a stabilizing heat flux. These parameterizations have not been sufficiently verified yet, however. Moreover, for the proper parameterization of these effects, it is important to understand clearly the roles of wave breaking and Langmuir circulation in the vertical mixing process in the ocean mixed layer.

Recently, Gemmrich and Farmer (1999) measured simultaneously the wave-enhanced turbulence and Langmuir circulation. However, it is very difficult to distinguish the roles of wave breaking and Langmuir circulation separately or to investigate the interaction between them based on the observation data because they usually occur simultaneously.

We are free to examine these effects separately in numerical simulations, however. One promising approach for this purpose is to use large eddy simulation (LES) that is able to simulate the three-dimensional turbulence structure of the ocean mixed layer. Moreover, a successful simulation of the ocean mixed layer by LES enables us to verify various assumptions used in ocean mixed layer models, as in the case of the LES of the atmospheric boundary layer (see, e.g., Ayotte et al. 1996; Noh et al. 2003a).

LES has been successful to simulate the atmospheric boundary layer to a high level of reality. On the other hand, the development of an appropriate LES model for the ocean mixed layer has been hindered by the difficulty of handling the boundary condition at the sea surface, in which wave breaking and Langmuir circulations are present, although pioneering works have been attempted recently (Siegel and Domaradzki 1994; Skyllingstad and Denbo 1995, 2001; Skyllingstad et al. 1999, 2000; Skyllingstad 2000; Wang et al. 1996, 1998; Wang and Müller 2002; McWilliams et al. 1997; McWilliams and Sullivan 2000).

Some LES works of the ocean mixed layer include neither Langmuir circulation nor wave breaking (Siegel and Domaradzki 1994; Wang et al. 1996, 1998; Wang and Müller 2002). Meanwhile, Skyllingstad and Denbo (1995) and McWilliams et al. (1997) successfully reproduced Langmuir circulations in the ocean mixed layer in which the momentum equation is modified by including a vortex force and an additional advection by Stokes drift, following the theory by Craik and Leibovich (1976). However, no attempt has been made yet to include the effects of wave breaking in the LES of the ocean mixed layer.

In this paper we attempted to accomplish the LES of the ocean mixed layer in which both wave breaking and Langmuir circulation are realized. By carrying out the LES with or without each contribution, wave breaking and Langmuir circulation, we aimed to clarify their respective roles in the ocean mixed layer. We also compared the dissipation rate and the TKE flux at the surface with observation data to confirm the validity of the LES results. Last, we compared the LES results with the one-dimensional ocean mixed layer model (OMLM) by Noh and Kim (1999) and examined the vertical mixing process represented by the OMLM. We restricted the present paper to the case without stratification.

2. LES model and simulations

The LES model used in this study is developed based on the Parallelized LES Model, which has been extensively applied for the atmospheric boundary layer (Schröter et al. 2000; Raasch and Harbusch 2001; Weinbrecht and Raasch 2001; Noh et al. 2003a) and for the ocean deep convection (Raasch and Etling 1998; Noh et al. 2003b). Subgrid-scale turbulence is modeled according to Deardorff (1980). A prognostic equation is solved for the subgrid-scale TKE, which is used to parameterize the subgrid-scale fluxes. The horizontal boundaries are periodic, and a radiation condition is imposed at the lower boundary. Recently the code has been parallelized, and the performance of the new parallelized code is found to be excellent on an SGI/Cray-T3E with an almost linear speedup up to a very large number of processors (Raasch and Schröter 2001).

For application to the ocean mixed layer, several modifications were made. A free slip boundary condition is imposed at the surface. The momentum equation is modified by including a vortex force and an additional advection by the Stokes drift following the theory by Craik and Leibovich (1976), similarly to McWilliams et al. (1997) and Skyllingstad and Denbo (1995).

The major modification in the present LES is the inclusion of wave breaking. Understandably, wave breaking is an extremely complicated phenomenon whose realistic simulation requires a resolution much higher than that of LES. The simulation of wave breaking at the present level is also unlikely to produce a realistic turbulence structure as observed at the sea surface (Chen et al. 1999, Scardovelli and Zaleski 1999; Kunugi and Satake 2002).

However, as long as we are concerned with the dynamical process in the ocean mixed layer influenced by wave breaking rather than wave breaking itself, it may suffice if we can simulate the turbulence generated by wave breaking instead of simulating the wave breaking process directly. Therefore, in this paper we introduced the near-surface turbulence generated by wave breaking in the LES model by imposing a small-scale random velocity fluctuation at the sea surface whose velocity and length scales are consistent with the observed ones in the real ocean. In this way, we attempted to simulate the LES of a realistic ocean mixed layer in which both wave breaking and Langmuir circulation are present.

The modified filtered equation is then given by

$$\frac{\partial u_i}{\partial t} + (u_j + u_{sj})\frac{\partial u_i}{\partial x_j} = -\frac{1}{\rho_0}\frac{\partial p}{\partial x_i} - \varepsilon_{ijk} f_j (u_k + u_{sk}) + \varepsilon_{ijk} u_{sj}\omega_k - \frac{\partial}{\partial x_j}\tau_{ij} + F_i, \quad (3)$$

where τ_{ij} is the subgrid-scale Reynolds stress and F_i is a random forcing that represents the generation of small-scale turbulence by wave breaking.

The random forcing F_i must be designed to produce the turbulence with the integral length and time scales as l_0 and τ_0, corresponding to those of the near-surface small-scale turbulence generated by wave breaking. This can be achieved approximately by imposing uncorrelated random forcing at each horizontal grid point of the size l_0 and at each time step of the size τ_0. Note that the velocity fields separated by these length and time scales can be regarded as independent. This approach is somewhat analogous to the forcing by Briggs et al. (1996), who simulated the turbulent production generated by an oscillating grid by assigning a random forcing localized in the physical and spectral spaces.

It is also assumed that the random forcing F_i exists only at the surface ($z = 0$), and its magnitude is proportional to u_*. The random forcing F_i is then expressed as

$$F_i = \frac{\alpha u_*}{\tau_0} G(0;\, 1)(1 - \delta_{i3})\delta(z), \quad (4)$$

where α is a proportional constant, and $G(0; 1)$ is the Gaussian random function whose mean is 0 and variance is 1. Here the random forcing is imposed only on the horizontal velocity fields, and the vertical velocity is determined so as to satisfy continuity at the surface, that is, the rigid-lid surface.

The rate of energy input by the random forcing, I, can be obtained from (3) by $\overline{u_i(t)F_i(t)}\ \Delta z$. The discretized equation of (3) can be written in the form

$$u_i^{n+1} = u_i^n + K(u_i^n)\tau_0 + F_i\tau_0 \quad (5)$$

for the explicit formula, where $K(u_i^n)$ indicates the other terms combined. Further, in the discretized form, I can be approximated by $\overline{(u_i^n + u_i^{n+1})F_i^n}\Delta z/2$. Since the random forcing given at each time step is independent of the existing fluid field, I can be estimated as (Alvelius 1999)

$$I \cong \frac{1}{2}\overline{(F_i^n)^2}\tau_0\Delta z = \frac{(\alpha u_*)^2}{4\sqrt{\pi}\tau_0}\Delta z \quad (6)$$

by using $\overline{G^2} = 1/2\sqrt{\pi}$.

The value of $\alpha = 3.0$ was determined so that the profile of the resultant dissipation rate is consistent with the observed one (Agrawal et al. 1992; Craig and Banner 1994; Anis and Moum 1995; Drennan et al. 1996; Terray et al. 1996) (see section 3d). Various values were suggested for the roughness length scale at the surface in the range 0.1–8 m (Agrawal et al. 1992; Craig and Banner 1994; Drennan et al. 1996; Gemmrich and Farmer 1999). Accordingly, we assumed the length scale of turbulence at the surface as $l_0 = 1.25$ m in our model. The time scale of random forcing τ_0 was determined by $\tau_0 = 0.1 l_0/\alpha u_*$.

Based on the evaluation $\alpha = 3.0$, we are able to estimate the TKE flux at the surface as $I = mu_*^3$ with $m \cong 40$, which is comparable to the estimation by Craig and Banner (1994) such as $m \cong 100$.

There are also observational evidences suggesting that m is not constant but is a function of the wave field (Terray et al. 1996; Drennan et al. 1996; Gemmrich and Farmer 1999). However, the reliable data for the global wave field at the sea surface is not yet available, and none of the ocean mixed layer models incorporates its information so far. We regard that m is constant in the present simulation since one of the important objectives of the present LES is to examine the ocean mixed layer model.

For simplicity, we assumed that both the wind stress and wave fields are in the x direction and further assumed that the wave field is steady and monochromatic. The associated Stokes velocity is then given by

$$u_s = U_s \exp(-4\pi z/\lambda), \tag{7}$$

with $U_s = (\pi a/\lambda)^2(g\lambda/2\pi)^{1/2}$, where a is the wave height, λ is the wavelength, and g is the gravitational acceleration. For wave height and wavelength, we used typical values such as $a = 1.0$ m and $\lambda = 40$ m, which makes $U_s = 0.049$ m s^{-1}.

The model domain was 300 m in the horizontal direction (x and y) and 80 m in the vertical direction (z). The number of grid points was $240 \times 240 \times 64$, and the corresponding grid sizes were 1.25 m in both horizontal and vertical directions. The wind stress was given by a constant friction velocity $u_* = 0.01$ m s^{-1}, which results in $\mathrm{La}_t = 0.45$. Note that La_t is usually around 0.2–0.5 under quasi-equilibrium conditions of wind and waves (e.g., Smith 1992). A free-slip boundary condition was applied at the bottom. The Coriolis force was given by $f = 1.2 \times 10^{-4}$ s^{-1}, and the density was assumed to be constant.

The model was started from rest and a weak surface cooling was forced during the first 900 s to initiate the turbulent motion. The integration was carried out until the equilibrium was approached ($t = 8$ h).

To investigate the effects of wave breaking and Langmuir circulation in the ocean mixed layer, we carried out four different experiments (EXP): cases with both effects (EXP LB), with none of these effects (EXP O), with only wave breaking (EXP B), and with only Langmuir circulation (EXP L).

3. Results

a. The vertical velocity field

Figure 1 presents the instantaneous vertical velocity fields from four different experiments at horizontal cross sections with increasing depths ($z = 1.25$, 10, 25, and 50 m).

The effects of Langmuir circulation are clearly evidenced in the comparison of the cases EXP O and EXP L. In the presence of the vortex force (EXP L), streaks of the strong downwelling zone beneath the surface convergence appear parallel to each other, associated with the formation of Langmuir cells. Near the surface the stripes are longitudinally oriented along the direction of wind stress. With increasing depth, the direction of stripes spirals clockwise toward a diagonal orientation, implying the Coriolis effect. The downwelling velocity field is narrower and stronger than the upwelling one. The downward velocity increases typically up to 0.04 m s^{-1}. The distance between the stripes increases with depth, reaching about 100 m at $z = 25$ m. There appear instances of joining of convergence zones with Y junctions, as observed in the ocean (Thorpe 1992; Farmer and Li 1995). At $z = 50$ m the stripe pattern of the downwelling zone is more fragmented and diffused, suggesting that the vertical extent of Langmuir circulation is limited by the depth equivalent to the wavelength λ (=40 m). It is also observed that the orientation of stripes and the distance between them are not significantly changed anymore between $z = 25$ m and $z = 50$ m. These patterns are in good agreement with the previous LES results by Skyllingstad and Denbo (1995) and McWilliams et al. (1997).

On the other hand, in the absence of a vortex force (EXP O), no organized structure appears, although the velocity field is weakly aligned along the wind direction near the surface and rotates toward a diagonal direction with increasing depth. However, at $z = 25$ m the velocity field is more or less isotropic without any directional tendency. The downward velocity is weaker, and the upwelling and downwelling velocity fields are more symmetrical than in EXP L. It is also found that the length scale of eddies increases with depth here, which is consistent with the assumption used in most ocean mixed layer models.

In the presence of wave-breaking effects (EXP B and EXP LB), the velocity fields near the surface up to $z \sim 5$ m are dominated by much stronger small-scale turbulence generated by wave breaking, but the Langmuir circulation pattern below the near-surface zone remains relatively unaffected by the presence of wave breaking. It is consistent with the observational evidence that most turbulent kinetic energy generated by wave breaking is lost within a depth comparable to the amplitude of breaking waves, and thus the influence of wave breaking is normally confined to a layer that is a few meters thick near the sea surface (Rapp and Melville 1990; Melville 1994; Gemmrich and Farmer 1999). Gemmrich and Farmer (1999) also suggested that the flow field within the ocean mixed layer can be represented by the combination of the advection by Langmuir circulation and the small-scale near-surface mixing due to wave breaking.

Nevertheless, the Langmuir cells from EXP LB show a weak tendency of becoming less coherent than EXP L, and the stripe pattern almost disappears at $z = 50$ m. Accordingly, the downward velocity of downward jets becomes slightly weaker (see also Fig. 4). It may

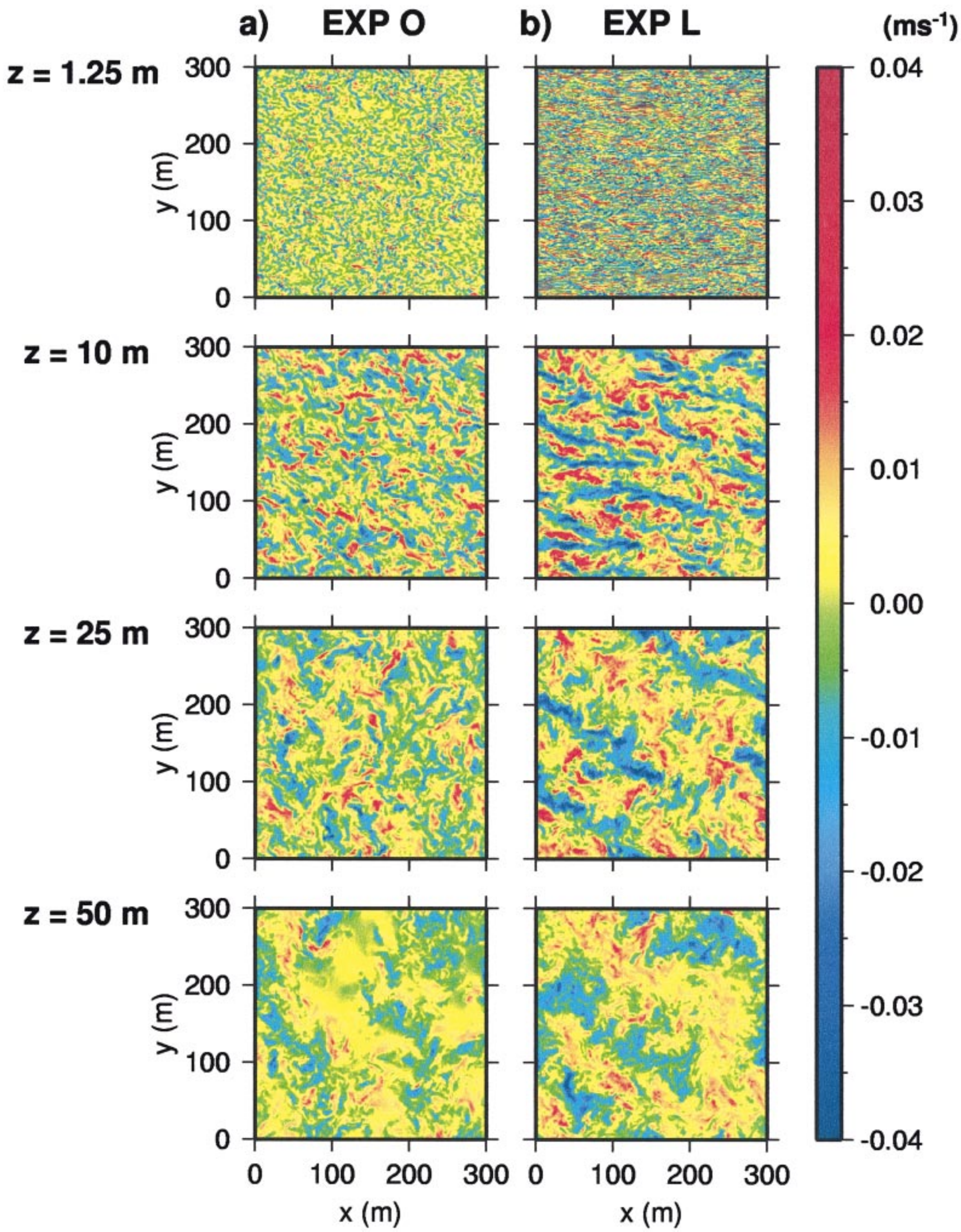

FIG. 1. Distributions of vertical velocity at the horizontal cross sections (z = 1.25, 10, 25, and 50 m): (a) EXP O, (b) EXP L, (c) EXP B, and (d) EXP LB.

be due to the fact that wave breaking disturbs the velocity field induced by the vortex force at the surface.

The distinctive features of the ocean mixed layer can be also clearly identified in the instantaneous vertical velocity fields in vertical cross sections (Fig. 2). In the case of EXP L, strong downward plumes associated with Langmuir circulation are clearly observed to a depth of about z = 50 m. We can also notice from Fig. 2 that the main reason for the increase of the distance between Langmuir cells, as observed in Fig. 1, is that the depths of penetration are different for different plumes.

We observed a similar pattern from EXP LB except near the surface, although the plumes from EXP LB tend to be less coherent and penetrate to less depth in comparison with those from EXP L, consistent with the horizontal view of Fig. 1.

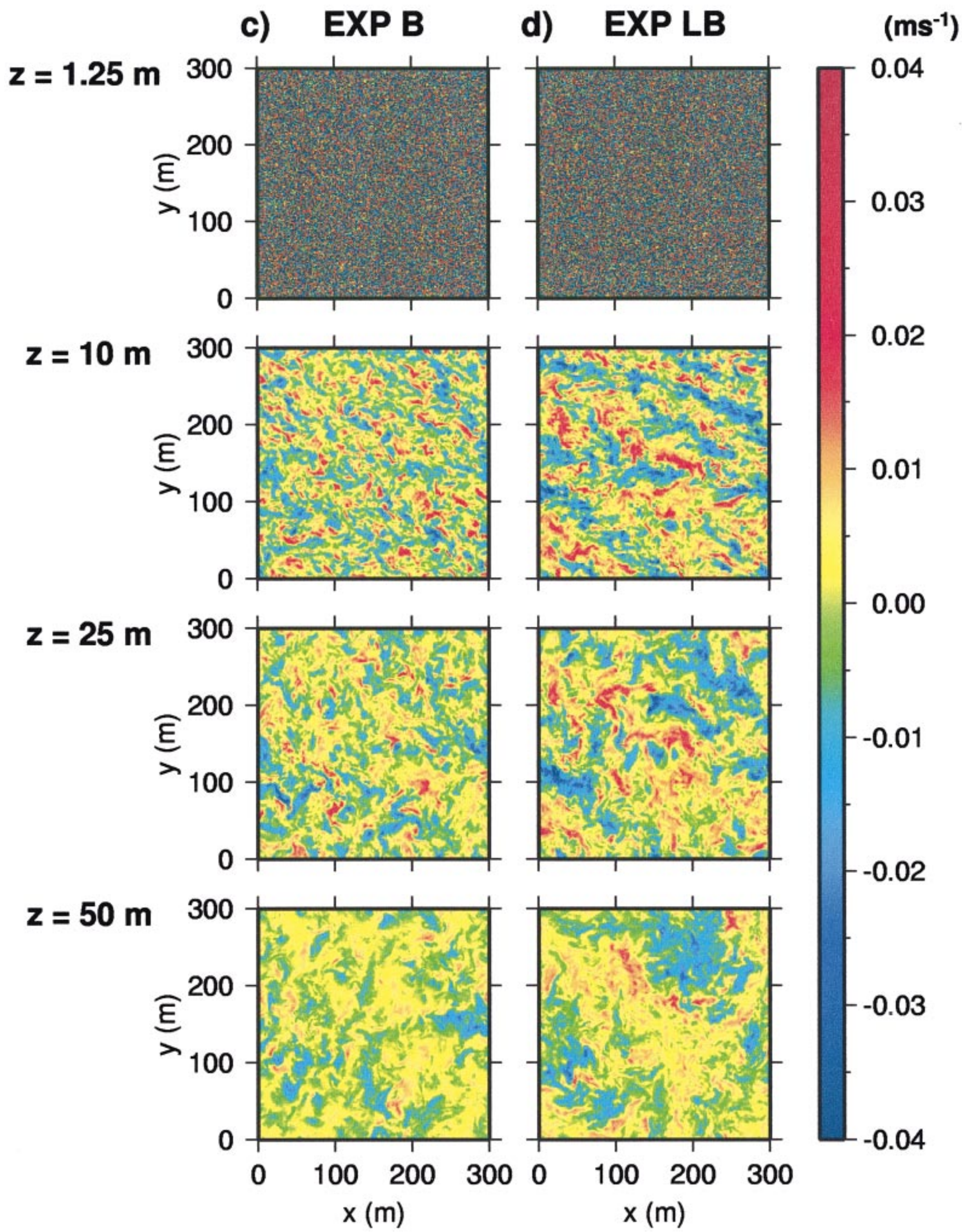

FIG. 1. (*Continued*)

On the other hand, in the absence of a vortex force (EXP O and EXP B), coherent downward plumes, penetrating up to a certain depth, do not appear contrary to the cases of EXP L and EXP LB. The intensity of the velocity becomes weaker rapidly with depths. The result from EXP B is not significantly different to those from EXP O, except for the presence of strong small-scale turbulence near the surface.

b. *Spectrum of the vertical velocity field*

Figure 3 compares horizontal spectra of the vertical velocity field Φ_w at various depths in the ocean mixed layer (z = 1.25, 2.5, 7.5, 12.5, 25, and 50 m), obtained from the four different experiments (EXP O, EXP L, EXP B, and EXP LB).

As expected, the small-scale turbulence dominates

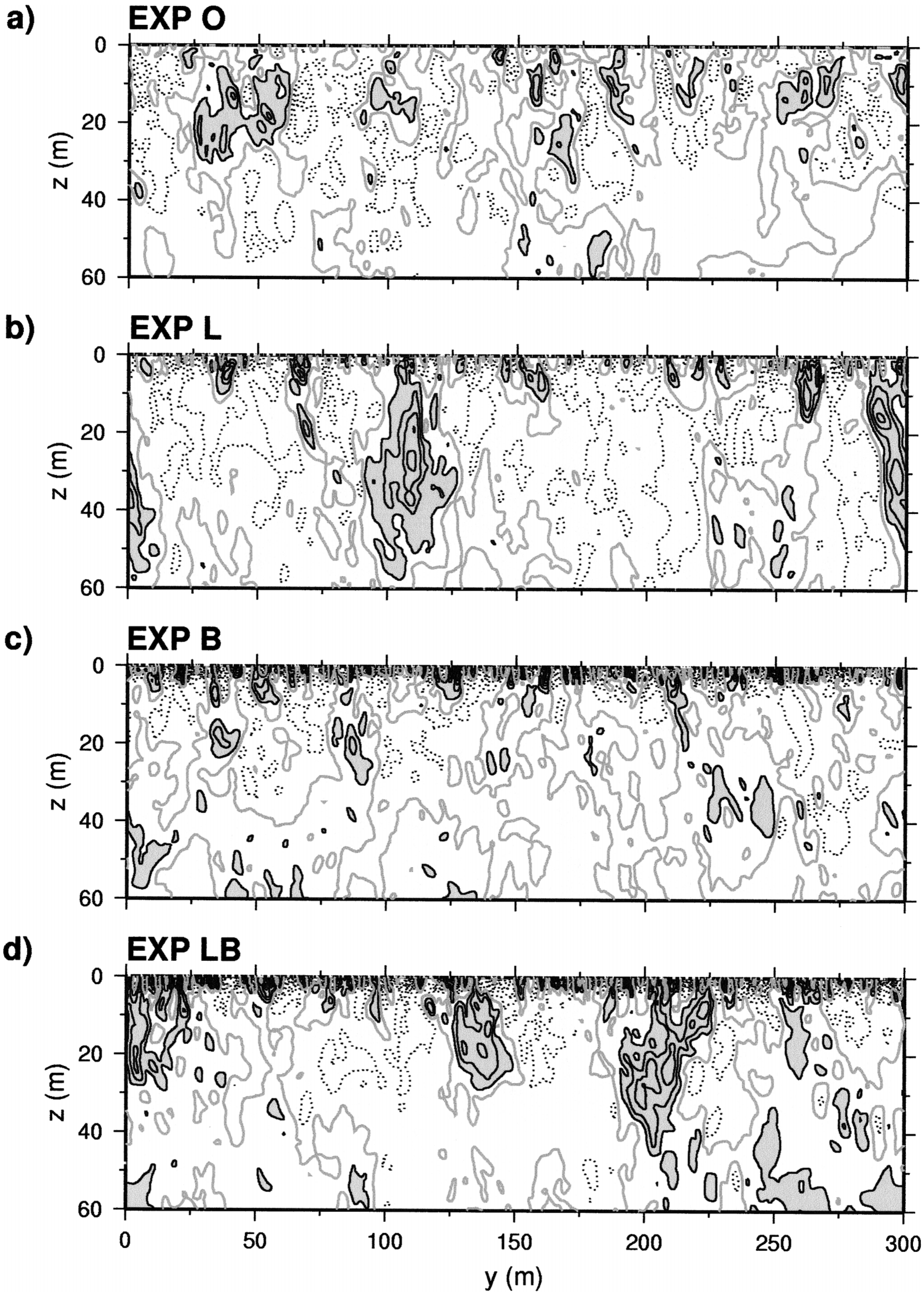

FIG. 2. Distributions of vertical velocity at the vertical cross sections. Contour levels are 0.01 m s^{-1}. Solid lines represent the downward velocity, and dotted lines represent upward velocity. Regions in which the downward velocity exceeds 0.01 m s^{-1} are shaded; (a) EXP O, (b) EXP L, (c) EXP B, and (d) EXP LB.

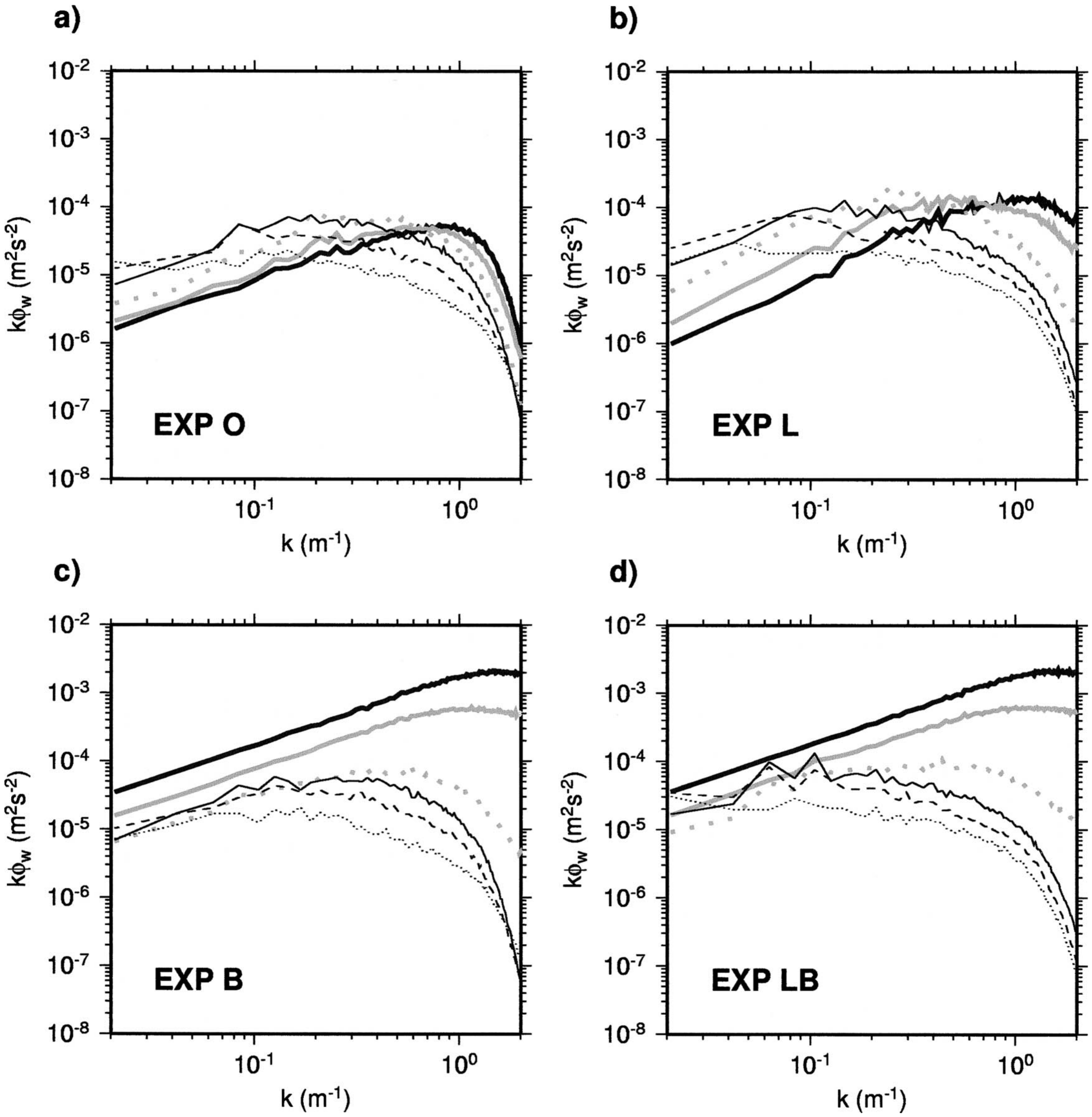

FIG. 3. Horizontal wavenumber spectra of the vertical field Φ_w at various depths in the ocean mixed layer (thick solid: $z = 1.25$ m, thick shaded: 2.5 m, shaded dots: 7.5 m, thin solid: 12.5 m, dashed: 25 m, and dotted: 50 m): (a) EXP O, (b) EXP L, (c) EXP B, and (d) EXP LB.

near the surface in the presence of wave breaking, but it does not affect significantly the spectra below the near-surface zone. It is consistent with the observation by Lien et al. (1998) and D'Asaro and Lien (2000) that Lagrangian frequency spectra of vertical velocity have similar shapes in spite of widely different conditions of wave breaking at the sea surface.

It is interesting, however, to observe that the level of small-scale turbulence near the surface also increases substantially by the presence of Langmuir circulation (EXP L), as pointed out by Skyllingstad and Denbo (1995) and McWilliams et al. (1997).

In the deeper layer ($z = 7.5$, 12.5, 25, and 50 m), the levels of the spectra at low wavenumbers in EXP L and EXP LB are substantially higher than those of EXP O and EXP B as a result of large-scale eddies associated with the Langmuir circulation. For example, the spectra at $z = 12.5$ m from EXP L and EXP LB show values that are about 2 times as large as those from EXP O and EXP B near $k \sim 0.1$ m^{-1}. The levels of the spectrum of EXP LB at these depths are slightly lower than those of EXP L, suggesting that Langmuir circulations are weaker in the former, as mentioned in the previous section.

The inertial subrange of the spectrum, which follows the Kolmogorov spectrum $k\Phi_w \propto \varepsilon^{2/3}k^{-2/3}$, appears in the spectra at depths below $z = 7.5$ m for all experiments, thus confirming the premise of LES. On the other

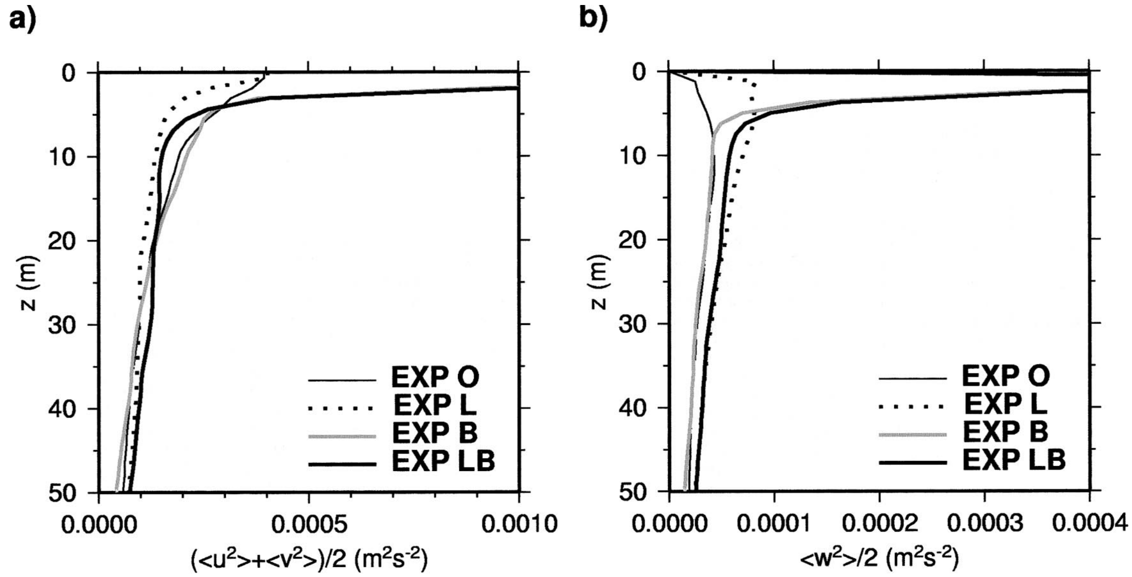

FIG. 4. Profiles of the mean horizontal (a) TKE and the mean vertical (b) TKE from each experiment. Here the maximum values of the mean horizontal and vertical TKE near the surface, which are cut off in figures, reach 0.006 and 0.001, respectively, for both EXP B and EXP LB.

hand, in the near-surface zone, where small-scale turbulence generated by wave breaking dominates, the inertial subrange does not appear within the grid resolution of the present simulation. Note that the grid size is not sufficient to resolve small eddies near the surface in the LES of the atmospheric boundary layer either.

c. *Mean profiles of turbulent kinetic energy and velocity*

The effects of wave breaking and Langmuir circulation on the structure of the ocean mixed layer can be clearly noticed in the vertical profiles of the mean horizontal and vertical turbulent kinetic energies (TKE) (Fig. 4) and of the mean horizontal velocities (Fig. 5). The horizontal mean profiles from LES were obtained by averaging over 600 s.

The strong enhancement of TKE in both horizontal and vertical directions appears in the presence of wave breaking near the surface in EXP B and EXP LB, but it is generally limited to the depth of about 5 m, as expected from Figs. 1, 2, and 3.

On the other hand, a significant increase of the vertical TKE is observed over almost the entire depth of the ocean mixed layer in the presence of Langmuir circulation (EXP L and EXP LB). It reflects the influence of the strong downward jets associated with Langmuir circulation, as observed in Figs. 1 and 2. It is also found that the horizontal TKE is decreased in the upper layer in the range of z = 5–20 m, when it is influenced by Langmuir circulation. This may be attributed to the fact that the velocity shear is decreased substantially in the presence of Langmuir circulation (EXP L and EXP LB), as shown in Fig. 5, thus resulting in a reduced shear production.

The vertical TKE below the near-surface zone is slightly smaller in the presence of wave breaking (EXP LB) than the case without wave breaking (EXP L), reflecting the weakened Langmuir circulation in the presence of wave breaking, as shown in Figs. 1, 2, and 3.

The enhancement of TKE near the surface in the presence of wave breaking contributes to the decrease of the velocity gradient near the surface in EXP B in comparison with EXP O, as shown in Fig. 5. However, very effective vertical mixing of momentum occurs down to much deeper depths in the presence of Langmuir circulation, and the velocity shear almost disappears in the ocean mixed layer (EXP L and EXP LB). Further, it is found that the surface current in the Ekman layer is oriented farther away from the wind, when Langmuir circulations are present (EXP L and EXP LB).

The characteristics of the profiles from EXP O and EXP L are in good agreement with McWilliams et al. (1997) with regard to the effects of Langmuir circulation.

d. *Mean profiles of dissipation rate*

Numerous field experiments carried out during the last few years to measure the dissipation rate of turbulence ε in the upper ocean have confirmed that wave breaking causes the value of ε near the sea surface to be ~two orders of magnitude larger than expected from the classical logarithmic boundary layer near a rigid wall (Agrawal et al. 1992; Anis and Moum 1995; Drennan et al. 1996; Melville 1996; Terray et al. 1996). Accord-

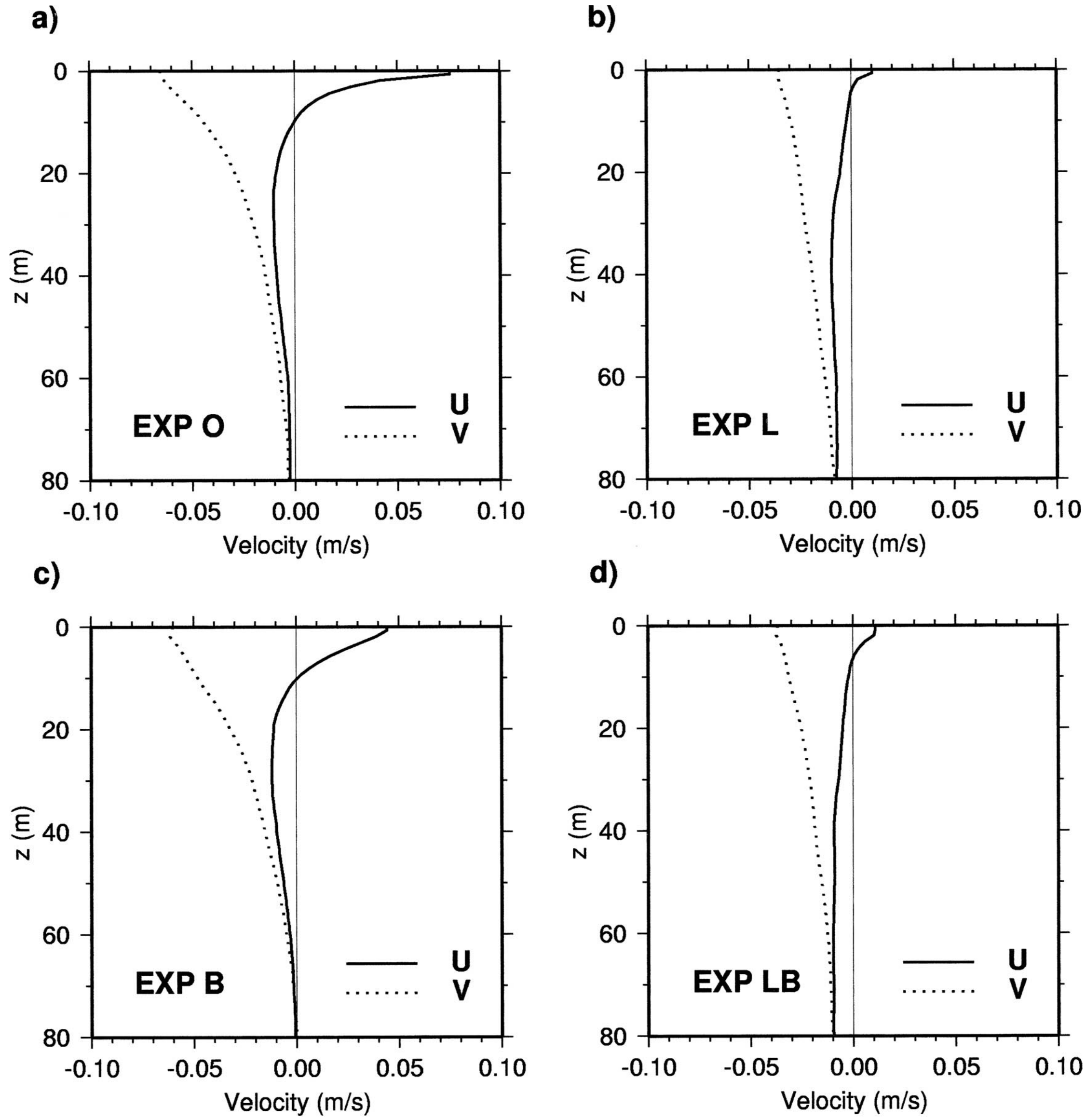

FIG. 5. Profiles of the mean horizontal velocities: (a) EXP O, (b) EXP L, (c) EXP B, and (d) EXP LB.

ingly, the relation for the variation of ε with depth z appears as $\varepsilon \sim z^{-n}$ with $n \sim$ 2–4 near the surface, in contrast to the wall boundary layer in which $\varepsilon \sim z^{-1}$, while the law-of-the-wall boundary layer may be recovered away from the near-surface zone.

For example, Craig and Banner (1996) suggested that the dissipation rate near the surface is estimated as

$$\varepsilon = \frac{2.4Au_*^3}{z_0}\left(1 + \frac{z}{z_0}\right)^{-3.4}, \tag{8}$$

while it approaches the scaling of the logarithmic boundary layer based on the surface wind stress, namely,

$$\varepsilon = \frac{u_*^3}{\kappa z}, \tag{9}$$

as the distance from the surface increases, where κ is the von Kármán constant. Here the proportional constant A in (8) was provided as $A = 0.5C_p/u_*$ by Terray et al. (1996), where C_p is the phase velocity of the dominant surface waves.

Previous LES experiments of the ocean mixed layer did not include the effects of wave breaking, and therefore underestimated the dissipation rate near the surface. For example, Skyllingstad et al. (1999) compared the estimation of the observed dissipation rate (8) with LES data and found that in the upper few meters the dissipation rate from LES underestimates the estimation from (8) by more than an order of magnitude.

We repeated the comparison in order to investigate the effects of wave breaking using our LES data. Figure

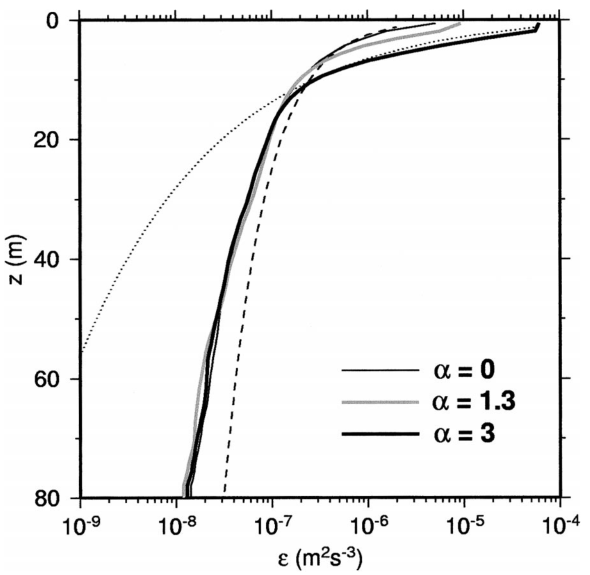

FIG. 6. Profiles of the dissipation rates [dashed: the scaling for the wall layer (9), dotted: the scaling by Craig and Banner (1994) (8), thin solid: LES ($\alpha = 0$), thick shaded: LES ($\alpha = 1.3$), and thick solid: LES ($\alpha = 3.0$)].

6 compares the profiles of dissipation rates with the estimation of the observation data (8) given by Craig and Banner (1994) as well as the scaling of the logarithmic boundary layer of (9). For the roughness depth z_0 in (8), we assumed the typical value as used in Skyllingstad et al. (1999) ($z_0 = 1$ m). We compared the profiles of dissipation rate with three different values of α in (4), which represents the contribution of wave breaking in the production of turbulence; that is, $\alpha =$ 0, 1.3, and 3.0.

For the case of $\alpha = 0$, which corresponds to the case of Skyllingstad et al. (1999), we found, likewise, that the LES data underestimate the dissipation rate by more than an order of magnitude. As the value of α increases, the dissipation rate increases accordingly in the near-surface zone up to a few meters, while it remains unaffected in the deeper layer. The close agreement with the observation data is found when $\alpha = 3.0$. Therefore, we used this value of α in the present paper to represent the generation of small-scale turbulence by wave breaking.

The scaling by Craig and Banner (1994) itself may have uncertainty, as pointed out by Drennan et al. (1996). It is important, however, to notice that the present simulation reproduces well the general characteristic of the profiles of the dissipation rate in the ocean mixed layer; that is, the value of ε near the sea surface to be $\sim$two orders of magnitude larger than that near a rigid wall, while recovering the law-of-the-wall boundary layer away from the near-surface zone.

4. Comparison with an ocean mixed layer model

a. The ocean mixed layer model (Noh model)

In the horizontally homogeneous ocean mixed layer without stratification, the mean velocities U and V and the mean TKE E are given in the OMLM (Noh and Kim 1999; Noh et al. 2002) as follows:

$$\frac{\partial U}{\partial z} = \frac{\partial}{\partial z}\left(K\frac{\partial U}{\partial z}\right) + fV, \tag{10}$$

$$\frac{\partial V}{\partial z} = \frac{\partial}{\partial z}\left(K\frac{\partial V}{\partial z}\right) + fU, \quad \text{and} \tag{11}$$

$$\frac{\partial E}{\partial t} = \frac{\partial}{\partial z}\left(K_E\frac{\partial E}{\partial z}\right) + K\left[\left(\frac{\partial U}{\partial z}\right)^2 + \left(\frac{\partial V}{\partial z}\right)^2\right] - \varepsilon. \tag{12}$$

Here the eddy viscosity, the eddy diffusivity for TKE, and the dissipation rate are formulated as

$$K = Sql, \tag{13}$$

$$K_E = S_E ql, \quad \text{and} \tag{14}$$

$$\varepsilon = Cq^3/l, \tag{15}$$

with empirical constants $S = 0.39$, $S_E = 0.2$, and $C = 0.06$, where q is the rms turbulent velocity $[=(2E)^{1/2}]$ and l is the length scale of turbulence.

The surface boundary conditions for the mean velocities are given by

$$K\frac{\partial U}{\partial z} = \frac{\tau_x}{\rho} \quad \text{and} \quad K\frac{\partial V}{\partial z} = \frac{\tau_y}{\rho}, \tag{16}$$

where τ_x and τ_y are the wind stresses in the x and y directions and ρ is the density of seawater. Equations (10)–(16) are common in most ocean mixed layer models of turbulence closure type using the eddy viscosity (see, e.g., Mellor and Yamada 1982).

However, Noh and Kim (1999) took into consideration the effects of wave breaking by suggesting much larger values for the TKE flux and the length scale at the sea surface than those used in the atmospheric boundary layer. That is, the TKE flux and the length scale at the surface are represented as

$$K_E\frac{\partial E}{\partial z} = mu_*^3, \quad \text{and} \tag{17}$$

$$l = \frac{\kappa(z + z_0)}{1 + \kappa(z + z_0)/h}, \tag{18}$$

where h is the depth of the ocean mixed layer and κ is the von Kármán constant. Noh and Kim (1999) suggested the values as $m = 100$ and $z_0 = 1$ m, which is consistent with Craig and Banner (1994). Here we adjusted the proportional constant m as $m = 40$ according to the estimation by (5).

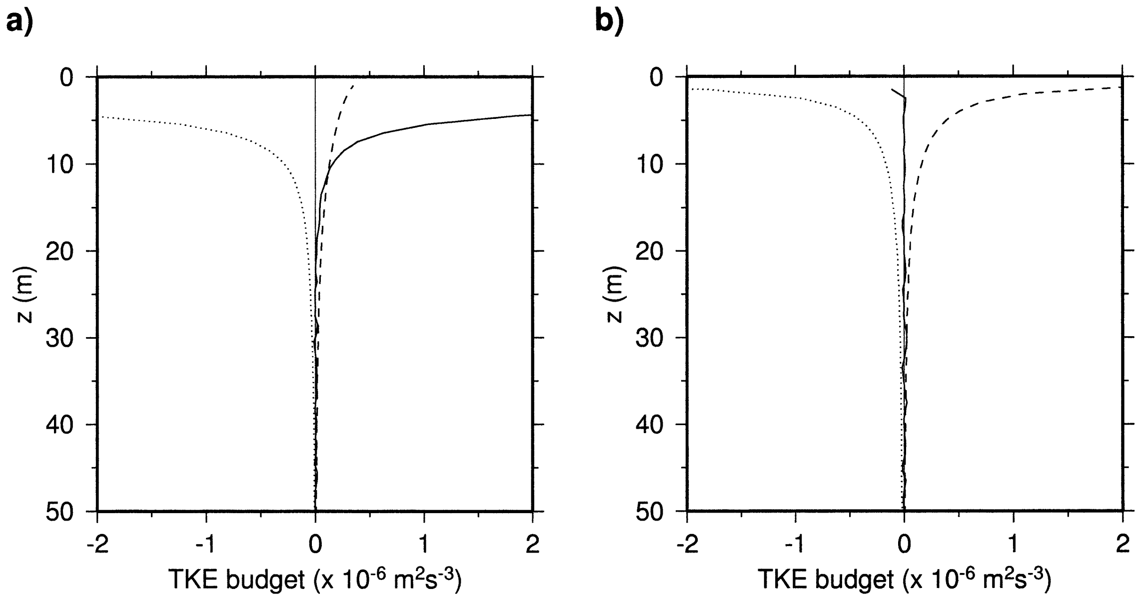

FIG. 7. Profiles of the terms of TKE budget from the OMLM (solid: TKE flux, dashed: shear production, and dotted: dissipation rate): (a) $m = 40$, $z_0 = 1$ m, and (b) $m = 0$, $z_0 = 0$ m.

b. The TKE budget

It has been suggested by Craig and Banner (1994) based on the analysis of the observation data that the enhancement of the TKE flux at the surface owing to wave breaking renders the downward TKE flux dominant in the TKE budget of the upper mixed layer, contrary to the case of the atmospheric boundary layer where shear production dominates.

For example, the profiles of TKE budget, obtained from the OMLM with wave breaking ($m = 40$, $z_0 = 1$ m) and without it ($m = 0$, $z_0 = 0$ m), clearly evidence the contrasting features mentioned above (Fig. 7).

Taking the above results into account, we examined the TKE budgets obtained from the four different LES experiments (EXP O, EXP L, EXP B, and EXP LB), as shown in Fig. 8. The results from EXP O and EXP B clearly show the dominance of the shear production and the TKE flux in the TKE budget of the upper mixed layer, respectively, in good agreement with the OMLM results shown in Fig. 7.

Meanwhile, Langmuir circulation is found to suppress shear production even further, as we can expect from Fig. 5. Under the influence of Langmuir circulation, the shear production almost disappears below the depth of a few meters (Figs. 8b and 8d). For the case with only wave-breaking effects (EXP B) (Fig. 8c), or correspondingly the case from the OMLM (Fig. 7a), the small contribution from shear production persists below the near-surface zone.

This supports the suggestion that the Langmuir circulation is largely responsible for the maintenance of the well-mixed condition of the ocean mixed layer (Leibovich 1983). The lack of the consideration of the effects of wave breaking and Langmuir circulation may also explain the reason why most ocean mixed layer models based on the turbulence closure using the eddy viscosity yield too strong shear (e.g., Mellor and Yamada 1982), contrary to the observation and the bulk ocean mixed layer models based on it (e.g., Niiler and Kraus 1977).

c. Comparison of the profiles of the mean velocity, TKE, and their fluxes

From the profiles of the mean velocity (Fig. 5) and the TKE budget (Fig. 8), we have observed that the velocity shear is substantially reduced in the presence of Langmuir circulation. The present OMLM does not take into account the effects of Langmuir circulation, and thus may still overestimate the velocity shear in the ocean mixed layer, although it reduces the velocity shear significantly near the surface by including the effects of wave breaking, as shown in Fig. 7.

Figure 9 compares the profiles of the velocity gradient and the momentum flux from the OMLM and the LES (EXP LB). The magnitude of the mean velocity shear decreases more rapidly and the momentum flux penetrates deeper in the LES data than in the OMLM result. It suggests that large eddies associated with Langmuir circulation are highly effective in transferring momentum downward. Note that the maximum velocity gradient appears below the surface in the profiles from the LES since the strong turbulence helps to maintain a rather uniform velocity profile near the surface (see also Fig. 5d).

Meanwhile, the profiles of mean TKE and the TKE

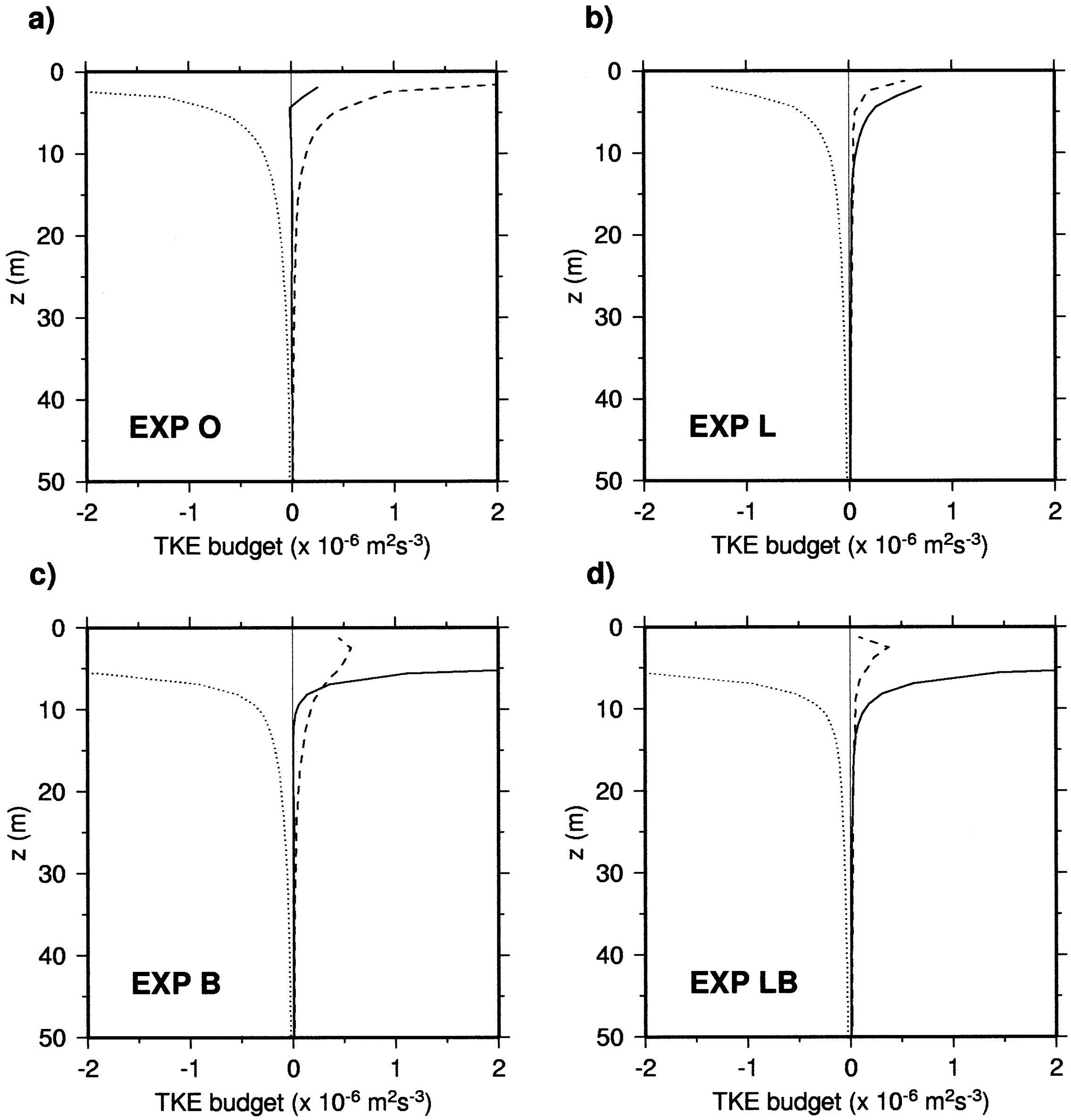

FIG. 8. Profiles of the terms of TKE budget from the LES (solid: TKE flux, dashed: shear production, and dotted: dissipation rate): (a) EXP O, (b) EXP L, (c) EXP B, and (d) EXP LB.

flux do not show significant discrepancy between the LES data from EXP LB and the OMLM results, although the LES results tend to penetrate deeper (Fig. 10).

Here the profiles of the momentum flux, TKE, and the TKE flux incorporate both the resolved and subgrid-scale components. It is noticed that the subgrid-scale part remains much smaller than the resolved part near the surface, unlike the case of the atmospheric boundary layer.

5. Conclusions

In this paper we attempted for the first time to perform a large eddy simulation (LES) of the ocean mixed layer in which both wave breaking and Langmuir circulation are realized. For the realization of the Langmuir circulation, we applied the theory by Craik and Leibovich (1976), similarly to the previous LES works by Skyllingstad and Denbo (1995) and McWilliams et al. (1997).

Coping with the difficulty in directly simulating the realistic wave breaking at the sea surface, however, we reproduced the turbulence field generated by wave breaking by forcing the small-scale random fluctuation of velocity at the sea surface. We presumed that the generated turbulence field is representative of that generated by wave breaking at the sea surface, when its length scale and dissipation rate are consistent with the

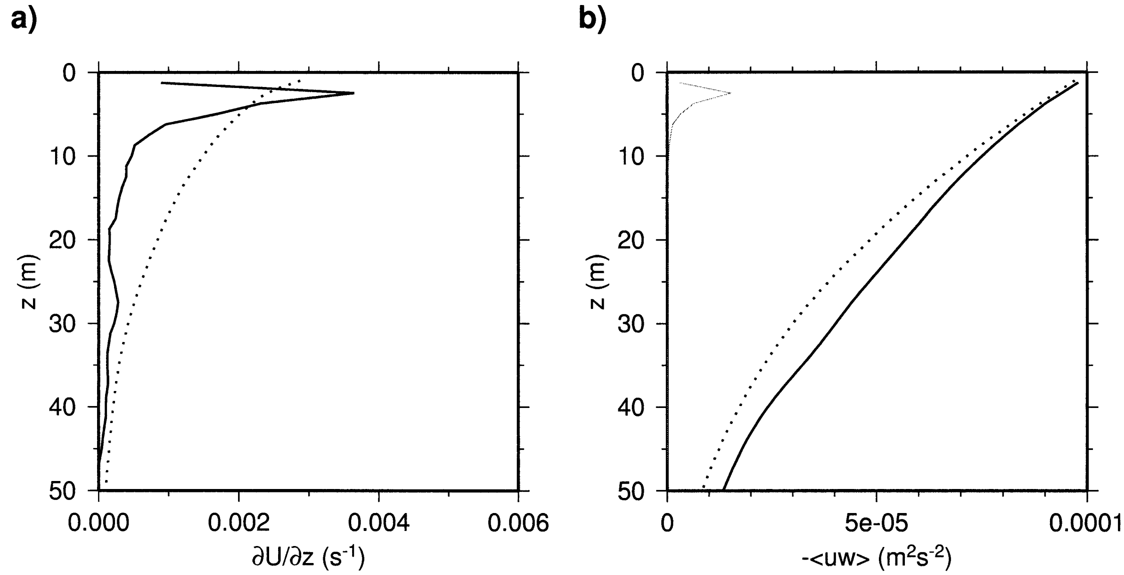

FIG. 9. Comparison of the profiles from the OMLM and the LES (solid: LES and dotted: OMLM). Thin solid lines are the contribution from the subgrid-scale motion: (a) $\partial U/\partial z$ and (b) $\overline{uw}$.

observed turbulence field near the sea surface. The resultant TKE flux at the surface turns out to be within the range of the observation data in the present LES, which helps to convince us of the appropriateness of the present approach.

It should be mentioned that a similar approach has been taken for the development of the LES of the atmospheric boundary layer. For the LES of the atmospheric boundary layer, the Monin–Obukhov similarity is assumed for the profiles of horizontal velocities and temperature near the surface instead of reproducing these profiles by treating the complex processes at the boundary explicitly.

Admittedly, the present approach of simulating the turbulence generation by wave breaking is rather crude. However, our understanding of the structure of the near-surface turbulence itself is also still very limited, and accurate information is not yet available. We hope to elaborate on the random forcing in the future study by utilizing more accurate observation data, by reflecting the process of turbulence generation by wave breaking (Melville 1994; Melville et al. 2002), and possibly by

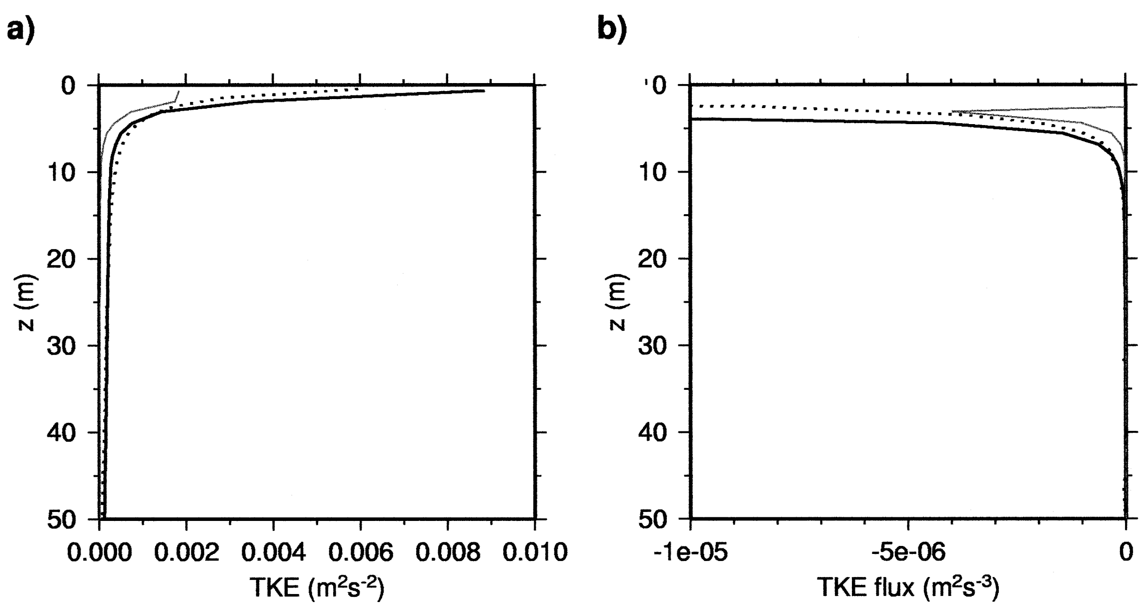

FIG. 10. Comparison of the profiles from the OMLM and the LES (solid: LES and dotted: OMLM). Thin solid lines are the contribution from the subgrid-scale motion: (a) TKE and (b) TKE flux.

including the information of wave fields (Terray et al. 1996; Drennan et al. 1996; Gemmrich and Farmer 1999).

Using the LES data from experiments with or without each contribution, that is, wave breaking and Langmuir circulation, we were able to clarify their respective roles in the ocean mixed layer, which is extremely difficult to perform in the real ocean. Moreover, we used the LES data to evaluate a one-dimensional ocean mixed layer model (Noh and Kim 1999; Noh et al. 2002) while investigating the effects of Langmuir circulation that is not included in the latter.

It was found that the effects of wave breaking are mainly limited to the near-surface zone of the upper few meters and the flow pattern below the near-surface zone is relatively unaffected. Meanwhile, Langmuir circulations become somewhat weakened and less coherent in the presence of wave breaking. One important effect of wave breaking is, however, that the turbulence production in the upper mixed layer becomes dominated by the TKE flux, whereas it is dominated by shear production in the absence of it, as in the case of the atmospheric boundary layer.

Large-scale eddies associated with Langmuir circulation turn out to be highly effective in transferring the momentum downward, and therefore help to maintain a well mixed layer without velocity shear. Accordingly, the velocity gradient from the OMLM is weaker near the surface and penetrates deeper, compared to the LES data.

The present result suggests that inclusion of the effects of Langmuir circulation may be important in the OMLM. In a future study, we hope to improve the OMLM by properly parameterizing the effects of Langmuir circulation based on more extensive LES data under various conditions including the stable and unstable ocean mixed layers.

Last, we mention that we repeated the same set of experiments (EXP O, EXP L, EXP B, and EXP LB) with two different combinations of wind stress and wave heights ($u_* = 0.007$ m s^{-1}, $a = 0.5$ m; $u_* = 0.012$ m s^{-1}, $a = 1.5$ m). Nevertheless, we have found that these experiments provide the same qualitative characteristics of the ocean mixed layer described in this paper, thus supporting the generality of the present results.

Acknowledgments. This work was supported by the Climate Environment System Research Center sponsored by the SRC program of KOSEF, the Ecotechnopia Project by KIEST, KISTI, and KORDI. Authors are grateful to Mr. W. G. Cheon for his help in setting up experiments.

REFERENCES

Agrawal, Y. C., E. A. Terray, M. A. Donelan, P. A. Hwang, A. J. Williams III, W. M. Drennan, K. K. Kahma, and S. A. Kitaigorodskii, 1992: Enhanced dissipation of kinetic energy beneath breaking waves. *Nature*, **359,** 219–220.

Alvelius, K., 1999: Random forcing of three-dimensional homogeneous turbulence. *Phys. Fluids*, **11,** 1880–1889.

Anis, A., and J. N. Moum, 1995: Surface wave–turbulence interaction: Scaling ε (z) near the sea surface. *J. Phys. Oceanogr.,* **25,** 2025–2045.

Ayotte, K. W., and Coauthors, 1996: An evaluation of neutral and convective planetary boundary-layer parameterisations relative to large eddy simulations. *Bound.-Layer Meteor.,* **79,** 131–175.

Briggs, D. A., J. H. Ferziger, J. R. Koseff, and S. G. Monismith, 1996: Entrainment in a shear-free turbulent mixing layer. *J. Fluid Mech.,* **310,** 215–241.

Burchard, H., 2001: Simulating the wave-enhanced layer under breaking waves with two-equation turbulence models. *J. Phys. Oceanogr.,* **31,** 3133–3145.

Chen, G., C. Kharif, S. Zaleski, and J. Li, 1999; Two-dimensional Navier–Stokes simulation of breaking waves. *Phys. Fluids,* **11,** 121–133.

Craig, P. D., and M. L. Banner, 1994: Modeling wave-enhanced turbulence in the ocean surface layer. *J. Phys. Oceanogr.,* **24,** 2546–2559.

Craik, A. D. D., and S. Leibovich, 1976: A rational model for Langmuir circulations. *J. Fluid Mech.,* **73,** 401–426.

D'Alessio, S. J. D., K. Abdella, and N. A. McFarlane, 1998: A new second-order turbulence closure scheme for modelling the ocean mixed layer. *J. Phys. Oceanogr.,* **28,** 1624–1641.

D'Asaro, E. A., and R. C. Lien, 2000: Lagrangian measurements of waves and turbulence in stratified flows. *J. Phys. Oceanogr.,* **30,** 2009–2022.

Deardorff, J. W., 1980: Stratocumulus-capped mixed layers derived from a three-dimensional model. *Bound.-Layer Meteor.,* **18,** 495–572.

Drennan, W. M., M. A. Donelan, E. A. Terray, and K. B. Katdaros, 1996: Oceanic turbulence dissipation measurements in SWADE. *J. Phys. Oceanogr.,* **26,** 808–815.

Farmer, D. M., and M. Li, 1995: Patterns of bubble clouds organized by Langmuir circulation. *J. Phys. Oceanogr.,* **25,** 1426–1440.

Gargett, A. E., 1989: Ocean turbulence. *Annu. Rev. Fluid Mech.,* **21,** 419–451.

Gaspar, P., 1988: Modeling the seasonal cycle of the upper ocean. *J. Phys. Oceanogr.,* **18,** 161–180.

Gemmrich, J. R., and D. M. Farmer, 1999: Near-surface turbulence and thermal structure in a wind-driven sea. *J. Phys. Oceanogr.,* **29,** 480–499.

Kraus, E. B., and J. S. Turner, 1967: A one-dimensional model of the seasonal thermocline. *Tellus,* **19,** 98–106.

Kunugi, T., and S. Satake, 2002: Direct numerical simulation of turbulent free surface flow with carbon-dioxide gas absorption. *Gas Transfer at Water Surfaces,* M. A. Donelan et al., Eds., Amer. Geophys. Union, 77–82.

Langmuir, I., 1938: Surface motion of water induced by wind. *Science,* **87,** 119–123.

Large, W. G., J. C. McWilliams, and S. C. Doney, 1994: Oceanic vertical mixing: A review and a model with a nonlocal boundary layer parameterization. *Rev. Geophys.,* **32,** 363–403.

Leibovich, S., 1977: Convective instability of stably stratified water in the ocean. *J. Fluid Mech.,* **79,** 715–743.

——, 1983: The form and dynamics of Langmuir circulation. *Annu. Rev. Fluid Mech.,* **15,** 391–427.

Li, M., and C. Garrett, 1997: Mixed layer deepening due to Langmuir circulation. *J. Phys. Oceanogr.,* **27,** 121–132.

Lien, R. C., E. A. D'Asaro, and G. T. Dairiki, 1998: Lagrangian frequency spectra of vertical velocity and vorticity in high-Reynolds number oceanic turbulence. *J. Fluid Mech.,* **362,** 177–198.

McWilliams, J. C., and P. P. Sullivan, 2000: Vertical mixing by Langmuir circulation. *Spill Sci. Technol. Bull.,* **6,** 225–237.

——, ——, and C. H. Moeng, 1997: Langmuir turbulence in the ocean. *J. Fluid Mech.,* **334,** 1–30.

Mellor, G. L., and P. A. Durbin, 1975: The structure and dynamics of the ocean surface mixed layer. *J. Phys. Oceanogr.,* **5,** 718–728.

——, and T. Yamada, 1982: Development of a turbulent closure model for geophysical fluid problems. *Rev. Geophys. Space Phys.,* **20,** 851–875.

Melville, W. K., 1994: Energy dissipation by breaking waves. *J. Phys. Oceanogr.,* **24,** 2041–2049.

——, 1996: The role of surface-wave breaking in air–sea interaction. *Annu. Rev. Fluid Mech.,* **28,** 279–321.

——, F. Veron, and C. J. White, 2002: The velocity field under breaking waves: Coherent structures and turbulence. *J. Fluid Mech.,* **454,** 203–233.

Niiler, P. P., and E. B. Kraus, 1977: One dimensional models of the upper ocean. *Modeling and Prediction of the Upper Layers of the Ocean,* E. B. Kraus, Ed., Pergamon Press, 143–172.

Noh, Y., 1996: Dynamics of diurnal thermocline formation in the ocean mixed layer. *J. Phys. Oceanogr.,* **26,** 2183–2195.

——, and H. J. Kim, 1999: Simulations of temperature and turbulence structure of the oceanic boundary layer with the improved near-surface process. *J. Geophys. Res.,* **104,** 15 621–15 634.

——, C. J. Jang, T. Yamagata, P. C. Chu, and C. H. Kim, 2002: Simulation of more realistic upper-ocean processes from OGCM with a new ocean mixed layer model. *J. Phys. Oceanogr.,* **32,** 1284–1507.

——, W. G. Cheon, S. Y. Hong, and S. Raasch, 2003a: Improvement of the K-profile model layer based on large eddy simulation data. *Bound.-Layer Meteor.,* **107,** 401–427.

——, ——, and S. Raasch, 2003b: The role of preconditioning in the evolution of open-ocean deep convection. *J. Phys. Oceanogr.,* **33,** 1145–1166.

Plueddemann, A. J., J. A. Smith, D. A. Farmer, R. A. Weller, W. R. Crawford, R. Pinkel, S. Vagle, and A. Gnanadesikan, 1996: Structure and variability of Langmuir circulation during the surface waves process program. *J. Geophys. Res.,* **101,** 3525–3543.

Price, J. F., R. A. Weller, and R. Pinkel, 1986: Diurnal cycling: Observations and models of the upper ocean response to diurnal heating, cooling and wind mixing. *J. Geophys. Res.,* **91,** 8411–8427.

Raasch, S., and D. Etling, 1998: Modeling deep ocean convection: Large eddy simulation in comparison with laboratory experiment. *J. Phys. Oceanogr.,* **28,** 1786–1802.

——, and G. Harbusch, 2001: An analysis of secondary circulations and their effects caused by small-scale surface inhomogeneities using large-eddy simulation. *Bound.-Layer Meteor.,* **101,** 31–59.

——, and M. Schröter, 2001: A large eddy simulation model performing on massively parallel computers. *Z. Meteor.,* **10,** 363–372.

Rapp, R. J., and W. K. Melville, 1990: Laboratory measurements of deep-water breaking waves. *Philos. Trans. Roy. Soc. London,* **331A,** 731–800.

Scardovelli, R., and S. Zaleski, 1999: Direct numerical simulation of free-surface and interfacial flow. *Annu. Rev. Fluid Mech.,* **31,** 567–604.

Schröter, M., J. Bange, and S. Raasch, 2000: Simulated airborne flux measurements in a LES generated convective boundary layer. *Bound.-Layer Meteor.,* **95,** 437–465.

Siegel, D. A., and A. Domaradzki, 1994: Large-eddy simulation of decaying stably stratified turbulence. *J. Phys. Oceanogr.,* **24,** 2353–2386.

Skyllingstad, E. D., 2000: Scales of Langmuir circulation generated using a large-eddy simulation model. *Spill Sci. Technol. Bull.,* **6,** 239–246.

——, and D. W. Denbo, 1995: An ocean large-eddy simulation of Langmuir circulations and convection in the surface mixed layer. *J. Geophys. Res.,* **100,** 8501–8522.

——, and ——, 2001: Turbulence beneath sea ice and leads: A coupled sea ice/large-eddy simulation study. *J. Geophys. Res.,* **106,** 2477–2498.

——, W. D. Smyth, J. N. Moum, and H. Wijesekera, 1999: Upper-ocean turbulence during a westerly wind burst: A comparison of large-eddy simulation results and microstructure measurements. *J. Phys. Oceanogr.,* **29,** 5–28.

——, G. B. Crawford, and W. D. Smyth, 2000: Resonant wind-driven mixing in the ocean boundary layer. *J. Phys. Oceanogr.,* **30,** 1866–1890.

Smith, J., 1992: Observed growth of Langmuir circulation. *J. Geophys. Res.,* **97,** 5651–5664.

Terray, E. A., M. A. Donelan, Y. C. Agrawal, W. M. Drennan, K. K. Kahma, A. J. Williams III, P. A. Hwang, and S. A. Kitaigorodskii, 1996: Estimates of kinetic energy dissipation under breaking waves. *J. Phys. Oceanogr.,* **26,** 792–807.

Thorpe, S., 1992: The break-up of Langmuir circulation and the instability of an array of vortices. *J. Phys. Oceanogr.,* **22,** 350–360.

Wang, D., and P. Müller, 2002: Effects of equatorial undercurrent shear on upper-ocean mixing and internal waves. *J. Phys. Oceanogr.,* **32,** 1041–1057.

——, W. G. Large, and J. C. McWilliams, 1996: Large-eddy simulation of the equatorial ocean boundary layer: Diurnal cycling, eddy viscosity, and horizontal rotation. *J. Geophys. Res.,* **101,** 3649–3662.

——, ——, and ——, 1998: Large-eddy simulation of the diurnal cycle of deep equatorial turbulence. *J. Phys. Oceanogr.,* **28,** 129–148.

Weinbrecht, S., and S. Raasch, 2001: High resolution simulations of the turbulent flow in the vicinity of an Arctic lead. *J. Geophys. Res.,* **106,** 27 035–27 046.

Weller, R. A., and J. F. Price, 1988: Langmuir circulation within the oceanic mixed layer. *Deep-Sea Res.,* **35,** 711–747.

Zedel, L., and D. M. Farmer, 1991: Organized structures in subsurface bubble clouds: Langmuir circulation in the open ocean. *J. Geophys. Res.,* **96,** 8889–8900.